International Symposium
On Turbulence and Shear Flow
Phenomena (TSFP-9)
June 30 - July 3, 2015 *Melbourne, Australia*

BLEED CONTROL OF PITCHING AIRFOIL AERODYNAMICS BY VORTICITY FLUX MODIFICATION

John M. Kearney and Ari Glezer
Woodruff School of Mechanical Engineering
Georgia Institute of Technology
Atlanta, Georgia, USA 30332-0405
jkearney@gatech.edu

ABSTRACT

Distributed active bleed driven by pressure differences across a pitching airfoil is used to regulate the vorticity flux over the airfoil's surface and thereby to control aerodynamic loads in wind tunnel experiments. The range of pitch angles is varied beyond the static stall margin ($14° < \alpha < 22°$) of the 2-D VR-7 airfoil at reduced pitching rates up to $k = 0.42$. Bleed is regulated dynamically using piezoelectric louvers between the model's pressure side near the trailing edge and the suction surface near the leading edge. The time-dependent interactions of the bleed with the cross flow and its effects on the production, accumulation, and advection of vorticity concentrations during the pitch cycle are measured using phase-locked PIV. These interactions mitigate the impact of abrupt transitions between attachment and separation by reducing the peak lift and moment loads that can lead to pitch instabilities. As a result, the stability of the pitch cycle can be improved (negative damping reduced) by as much as $\Delta E_\alpha = 1.21$ (at $k = 0.25$).

I. OVERVIEW

Aerodynamic bleed effected by pressure differences over a lifting surface interacts with the local surface vorticity layer to produce significant changes in vorticity flux and therefore in global aerodynamic forces and moments. Though passive bleed through porous surfaces for flow control was investigated as early as the 1920s (e.g., Lachmann, 1924) and since then by a number of researchers (e.g., Hunter, Viken, Wood, and Bauer, 2001, Han and Leishman, 2004, Lopera, Ng, and Patel, 2004), *active* distributed bleed by time-dependent regulation of surface porosity for mitigation of adverse aerodynamic effects on static and pitching airfoils has only been demonstrated recently by Kearney and Glezer (2012, 2013, 2014). These investigations revealed that such bleed can modify the formation and advection of surface vorticity concentrations and thereby alter the timing and strength of the dynamic stall vortex and aerodynamic loads during the pitch cycle.

Excursions in pitch through the static stall angle can result in high, transitory aerodynamic loads due to the rapid buildup and shedding of vorticity concentrations. When the pitch motion through stall is oscillatory (i.e., during dynamic stall), especially at rapid pitch rates ("reduced" frequencies of $k = \omega c/2U_\infty \gtrsim 0.1$), the alternating attachment and flow separation produce periodic forcing that can lead to structural instabilities that are manifested by severe torsion or flutter (Carta, 1967, Johnson and Ham, 1972, McCroskey, Carr, and McAlister, 1976, Ericsson and Reding, 1988). Therefore, the occurrence of dynamic stall on the retreating blade imposes limitations on rotorcraft forward flight speeds (Raghav and Komerath, 2013). The earlier work on dynamic stall has indicated that these adverse effects can be mitigated by modifying the evolution of the unsteady vorticity concentrations that arise due to the blade's motion.

The present investigations build on the earlier findings of Kearney and Glezer and focus on the time-dependent mechanisms by which bleed affects vorticity concentrations over the airfoil and in the near wake during oscillatory pitching. The alteration of the vorticity flux near the surface can have significant effects on the evolution and timing of the dynamic stall vortex that are manifested by changes in the lift hysteresis and pitch stability during the cycle.

II. EXPERIMENTAL SETUP AND PROCEDURES

The present investigation is conducted in a low-speed wind tunnel ($U_\infty = 15$ m/s, $Re_c = 190{,}000$) having a rectangular test section measuring 25 x 47 x 132 cm with optical access from all sides. The VR-7 airfoil model ($c = 20$ cm, $t_{max} = 0.12c$) spans nearly the entire width of the test section ($s = 24$ cm, with endplates). The model is mechanically isolated from the test section and is mounted on a shaft through $x/c = 0.25$. Dynamic pitch is driven by two synchronized, computer controlled servo motors, one on each side of the tunnel, that are each connected to the model through a load cell that measures lift and drag (within 0.011 N) and pitching moment (within 0.001 N·m), with frequency response of up to 500 Hz. The system can pitch the model sinusoidally at frequencies in excess of 25 Hz (corresponding to a reduced frequency of $k \approx 1$). High-resolution PIV measurements of the velocity field above the airfoil and in the near wake are obtained using a 1600 x 1200 pixel, 14-bit CCD camera and an Nd:YAG laser with cross stream views ranging in width from $0.1c$ to $0.6c$ (magnifications of 69 and 8 px/mm, respectively).

The airfoil model is fabricated using stereolithography (SLA) and includes several spanwise rows of low-resistance bleed ports through the pressure and suction surfaces that are open to the inner volume of the model (Figure 1). Each spanwise row is comprised of 16 10 mm-wide ports whose streamwise length increases with distance from the leading edge from 2 mm (at $x/c = 0$) to 2.5 mm (at $x/c = 0.95$). The bleed configuration in the present work leverages the pressure difference upstream of the trailing edge (on the pressure

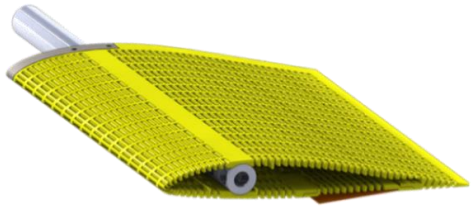

Figure 1. *Section view showing bleed passages in the upper and lower surfaces. The flow is regulated using cantilevered surface-mounted louvers on the pressure side (unused passages are sealed using thin tape).*

side) and the low pressure domain at the outlet on the suction surface near the leading edge ($0.03 < x/c < 0.04$). An array of planar piezoelectric louvers embedded over the inlet ports along the airfoil's span can be actuated at frequencies above 150 Hz to enable desirable time-varying bleed. As noted by Kearney and Glezer (2012), static displacement of the louvers varies nearly linearly with the applied voltage, and the effects of the louvers' presence on the aerodynamic characteristics of the airfoil in the absence of bleed (i.e. when the bleed passages are sealed) results in minimal interference and changes in aerodynamic loads.

III. VORTICITY FLUX MODIFICATION USING BLEED DURING PITCH

The earlier work of Kearney and Glezer demonstrated that the interaction of time-dependent bleed flow with the outer flow leads to temporal and spatial modulation of vorticity concentrations within the surface vorticity layer. In the present investigations, these effects are exploited to alter the dynamics of the formation and transport of vorticity concentrations associated with stall during the upstroke and flow reattachment during the downstroke.

The variations in $C_L(\alpha)$, $C_M(\alpha)$, and $C_D(\alpha)$ are measured phase-locked to the pitch cycle $\alpha(t) = 18° + 4°\cdot\sin(2U_\infty kt/c)$ (Figure 2a-c, respectively) for the base airfoil (gray) and with time-periodic bleed (red). In the absence of actuation, C_L increases and C_M decreases monotonically with α until the formation of the dynamic stall vortex begins near $\alpha = 20°$ (Figure 2a-b). This results in a rapid increase in C_L (up to 2.1 at $\alpha = 21°$) that is accompanied by an abrupt (nose-up) increase in C_M through $\alpha = 20°$ due in part to a traveling low-pressure zone associated with the dynamic stall vortex (e.g., McCroskey, Carr, and McAlister, 1976) and is followed by a steep decrease in C_M that continues almost through the maximum angle of the pitching cycle, $\alpha_{max} = 22°$. As the airfoil becomes fully stalled at α_{max}, C_L decreases rapidly ($\Delta C_L = -0.46$ by the beginning of the downstroke) and then continues to decrease through $C_{L,min} = 0.63$ at $\alpha = 14.7°$, when the flow begins to reattach and lift is restored. The onset of the downstroke and shedding of the dynamic stall vortex produce a rapid recovery of C_M, which increases throughout the downstroke segment of the pitch cycle to a slightly nose-up (CW) $C_M = 0.03$ at $\alpha = 14°$. The aerodynamic damping coefficient is $E_\alpha = -\frac{\int C_M d\alpha}{\pi\bar{\alpha}^2} = 0.05$ ($E_\alpha > 0$ indicates suppressive or stable damping). However, even though the cycle damping is slightly positive, the pitching cycle includes a CW loop ($19.5° < \alpha < 20.6°$) which is indicative of negative damping.

As shown in Figures 2a and b, the effect of the time-periodic bleed ($St_{act} = f_{act}c/U_\infty = 1.1$) at this pitch frequency is quite profound. Although there is a reduction in C_L during the upstroke compared to the base flow ($\Delta C_L \approx 0.25$), the rapid increase in C_L during the formation of the dynamic stall vortex is significantly muted, and the magnitude and rate of the decrease in C_L following the shedding of the dynamic stall vortex are significantly lower as well. Furthermore, the earlier flow attachment during the downstroke is associated with higher C_L for $20° > \alpha > 14°$. Therefore, the actuation results in a significant reduction in cycle hysteresis. Despite a reduction in lift during the upstroke, the cycle-averaged lift in the presence of bleed ($C_L = 1.26$) is not far from that of the base flow ($C_L = 1.31$). The corresponding changes in C_M are just as remarkable. The rapid variations that are associated with the shedding of the dynamic stall vortex are damped, and the increase in the nose-down rate during the upstroke is smaller than for the base flow. The maximum nose-down moment ($C_M = -0.30$) is lower in magnitude than for the baseline ($C_M = -0.35$) and occurs earlier during the pitch cycle ($\alpha = 21°$ compared to 21.7° for the base flow). Furthermore, $C_M(\alpha)$ is CCW throughout the entire pitch cycle indicating that the cycle is positively damped, and, in fact, $E_\alpha = 0.72$ which is significantly higher than in the base flow. In the presence of bleed, the drag is somewhat higher during the upstroke, but is lower near the maximum α ($C_{D,max} = 0.68$ at $\alpha = 21°$ compared to 0.80 for the base flow). During the downstroke, C_D is lower in the presence of bleed, resulting in a cycle-averaged difference relative to the base flow of 3%.

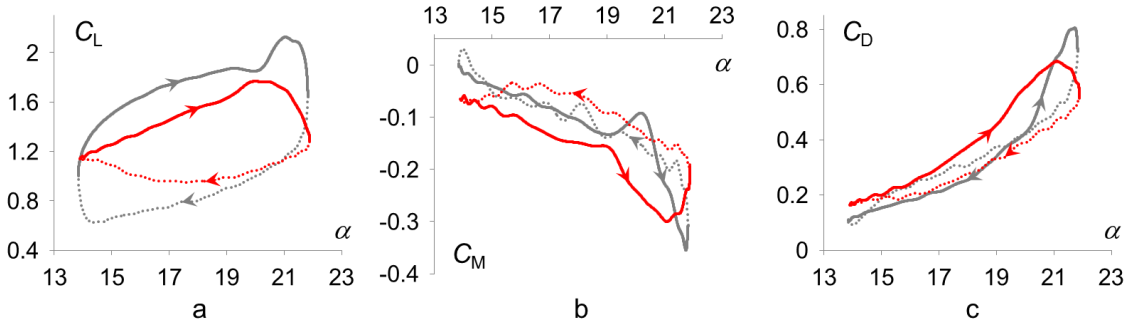

Figure 2. *Phase-averaged $C_L(\alpha)$ (a), $C_M(\alpha)$ (b), and $C_D(\alpha)$ (c) for $k = 0.17$ in the absence (—) and presence ($St_{act} = 1.1$, —) of bleed. Upstroke and downstroke motions are indicated by solid and dotted lines, respectively.*

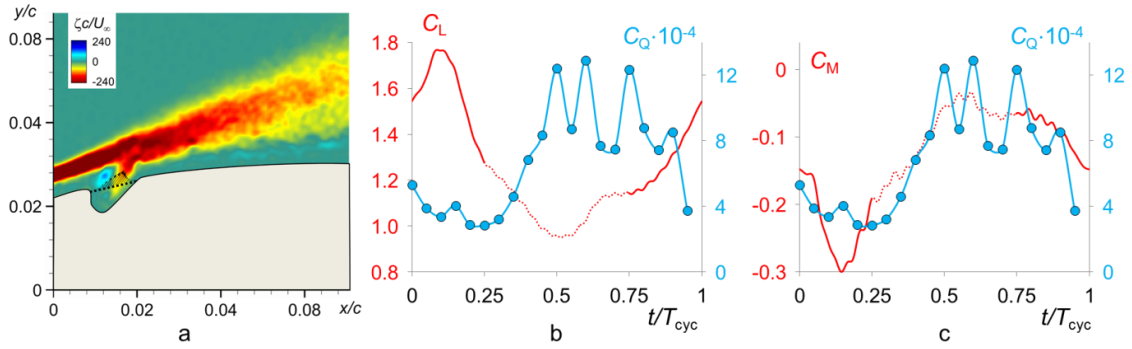

***Figure 3**. (a) Phase-averaged distribution of spanwise vorticity concentrations near the bleed outlet (on the suction surface, 0.03c downstream of the leading edge) at t/T_{cyc} = 0.45 during pitch oscillations (k = 0.17). The dashed line across the outlet (0.012 < x/c < 0.022) depicts the surface through which the bleed flow rate is calculated; (b, c) Phase-averaged variations of C_L (b) and C_M (c) during the pitch cycle (α = 18.0° during upstroke at t/T = 0) along with C_Q (—). The downstroke motion is indicated with dotted lines.*

The interaction between the time-periodic bleed flow issuing on the suction side, the outer flow, and the surface vorticity layer is investigated using phase-locked PIV measurements during the pitch cycle (k = 0.17). The evolution of the bleed flow near the outlet is shown in Figure 3a in a color raster plot of vorticity concentrations. At this instant, the airfoil is pitching down, α = 19.2°, and the components of the surface velocity are $u_{surface}$ = -0.027 m/s, and $v_{surface}$ = -0.071 m/s. The cross stream measurement domain is 0.01c by 0.01c and includes the bleed outlet (the airfoil's leading edge is located at x/c = -0.03). These data indicate that as a result of blockage by the bleed jet, the flow slows down upstream of the jet orifice and the boundary layer becomes thicker. The bleed flow is sufficient to lead to the deflection of the upstream boundary layer that is accompanied by the formation of a CCW vortex and the merging of the bleed jet with the shear layer of the deflected flow. Downstream of the bleed port, the flow separates and reversed flow and the formation of CCW vorticity concentration near the surface are evident for x/c > 0.02. The PIV measurements are used to estimate the phase-averaged bleed flow rate $C_Q = \frac{n \cdot s_{jet} \cdot \int \vec{V}_{jet} \cdot \vec{n}\, dl}{s \cdot c \cdot U_\infty}$ (where $n \cdot s_{jet}/s$ is fraction of the span occupied by the open bleed outlets). The flow rate is computed across the dashed line shown for reference in Figure 3a (0.012 < x/c < 0.022) in each of the phase-locked images.

As noted above, the bleed flow depends on the pressure difference between the inlet and outlet ports which can vary with angle of attack. Furthermore, the magnitude of the bleed flow rate is also regulated by the momentum of the cross flow over the outlet port. As shown in Figure 3b, the phase-averaged C_L (cf. Figure 2a), reaches a maximum when the flow is attached during the upstroke (C_L = 1.77, t/T_{cyc} = 0.10, where the cycle commences at α = 18.0° during upstroke), and has a local minimum during the downstroke (C_L = 0.95, t/T_{cyc} = 0.52) when the airfoil is stalled. However, the bleed flow rate has a minimum shortly after the maximum C_L (at t/T_{cyc} = 0.20) while the flow is still attached and a maximum at shortly after the minimum C_L (at t/T_{cyc} = 0.60) when the flow is stalled. These data indicate that the higher-momentum of the fully attached flow reduces (but does not completely prevent) significant penetration of the bleed into the cross flow, while the lower momentum when the flow is stalled enables higher bleed momentum flux. The oscillations in C_Q for 0.50 < t/T_{cyc} < 0.80 may be related to the periodic vortex formation and segmentation of the separating shear layer resulting from the self-regulating interaction with the outer flow (discussed in Kearney and Glezer, 2013), leading to reattachment during the downstroke. In contrast to Figure 3b, Figure 3c shows that the bleed flow tracks the pitching moment. During the upstroke, lower bleed flow is associated with the nose-down moment, and the bleed flow rate increases with C_M through t/T_{cyc} = 0.5, contributing to positive damping before undergoing oscillations through t/T_{cyc} = 0.9 that also appear (though to a lesser degree) in C_M.

The abrupt variations in aerodynamic forces and moments that result from the shedding of vorticity concentrations during the pitching cycle, particularly near α_{max} and α_{min}, are better understood by considering the timing and intensity of vorticity concentrations advecting into the near wake. Figure 4 shows 16 phase-locked measurements of spanwise vorticity concentrations and velocity distributions over a domain ranging from 0 < x/c < 0.57 and 0 < y/c < 0.92 (beginning at x/c = 0.05 downstream from the trailing edge) in the wake of the baseline airfoil spaced equally in time from 0 < t/T_{cyc} < 0.35 and 0.60 < t/T_{cyc} < 1. In Figure 4a (α = 18.0° on the upstroke, t/T_{cyc} = 0), concentrated layers of CW and CCW vorticity shed from the suction and pressure surfaces, respectively, before dissipating considerably by x/c = 0.20 due to interaction with the faster-moving freestream. While the interface of zero velocity gradient located between the opposite-sense vorticity layers is nominally aligned with the streamwise (x) axis, the convective effects of the dynamic pitching motion are observed in the "history" of the vorticity concentrations in the wake, i.e. the downward-vectoring of the layers between 0.15 < x/c < 0.55. The cross stream extent of the CW vorticity layer advecting from the suction side trailing edge increases slightly in Figure 4b (α = 19.2°, t/T_{cyc} = 0.05), as does the velocity deficit within the vorticity layers, marking the beginning of the reduction in CW flux that occurs prior to the shedding of the dynamic stall vortex. The roll-up of CW vorticity on the suction surface during dynamic stall is accompanied by a protrusion of the CCW vorticity layer that streams from the pressure side into the CW layer above (Figure 4c; α = 20.4°, t/T_{cyc} = 0.10), indicative of the shedding of a shear layer vortex preceding the dynamic stall vortex and coinciding with moment stall (cf. Figure 2b). As the dynamic stall vortex advects over the trailing edge and begins to enter the near wake (Figure 4d; α = 21.2°, t/T_{cyc} = 0.15), the CCW vorticity layer is vectored sharply downward (-11° relative to the freestream), C_M continues

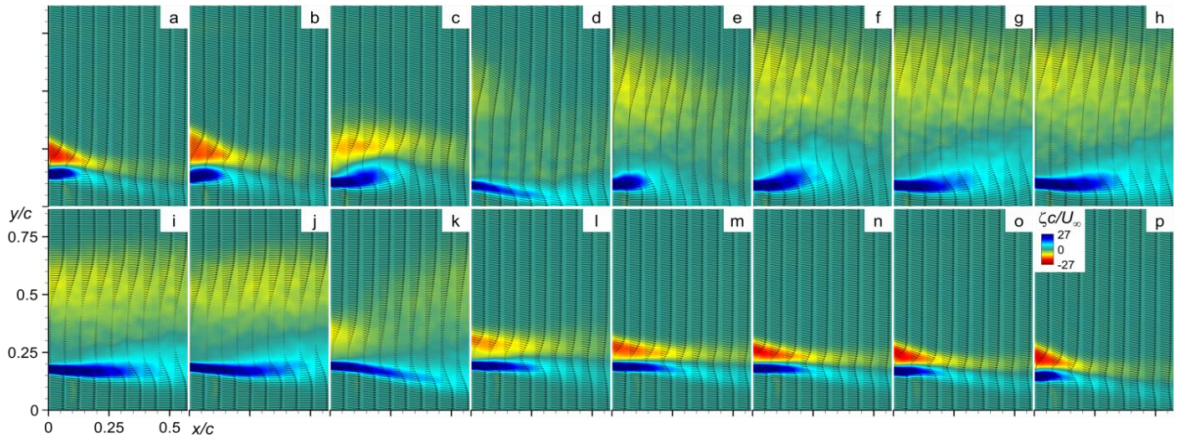

Figure 4. *Phase-locked measurements of spanwise vorticity and velocity in the wake (x/c = 0.05 downstream of the trailing edge) for the baseline airfoil during pitch oscillations from* $\alpha = 18° + 4°\cdot\sin(2\pi t/T_{cycle})$ *at k = 0.17:* $t/T_{cycle} = 0$ *(a), 0.05 (b), 0.10 (c), 0.15 (d), 0.20 (e), 0.25 (f), 0.30 (g), 0.35 (h), 0.60 (i), 0.65 (j), 0.70 (k), 0.75 (l), 0.80 (m), 0.85 (n), 0.90 (o), and 0.95 (p).*

to fall sharply ($dC_M/d\alpha \approx$ -0.19/°; cf. Figure 2b), and C_L begins a precipitous drop marked by massive leading-edge separation. The separated flow advects into the near wake in Figure 4e ($\alpha = 21.8°$, $t/T_{cyc} = 0.20$), shedding the low-pressure vortex and initiating a rebound in C_M from its minimum of -0.35. This is followed by spreading of CW vorticity concentrations across the upper portion of the measurement domain and a significant reduction in streamwise velocity through Figures 4f ($\alpha = 22.0°$, $t/T_{cyc} = 0.25$) and g ($\alpha = 21.8°$ on the downstroke, $t/T_{cyc} = 0.30$). The airfoil remains fully stalled during the majority of the downstroke, with recirculating flow evident from $0.20 < y/c < 0.45$ throughout and its wake narrowing only slightly from Figure 4h ($\alpha = 21.2°$, $t/T_{cyc} = 0.35$) to Figure 4i ($\alpha = 15.6°$, $t/T_{cyc} = 0.60$). Note that PIV frames corresponding to the downstroke motion during $0.35 < t/T_{cyc} < 0.65$, where the flow field remains similar to that of Figure 4i, are not shown here. The first evidence of reattachment (that progresses leading to trailing edge) is observed in the downward vectoring of the upstream CW vorticity concentration in Figure 4j ($\alpha = 14.8°$, $t/T_{cyc} = 0.65$), marking the minimum C_L level of 0.63. The CCW vorticity layer is further vectored downward in Figure 4k (to -7.5° relative to the freestream; $\alpha = 14.2°$, $t/T_{cyc} = 0.70$) along with the suction-side flow as reattachment reaches the trailing edge and the remnants of CW vorticity concentrations associated with stall are advected downstream. Once flow is fully attached, lift is rapidly recovered (cf. Figure 2a) and the concentrations of opposite-sense vorticity stretching into the wake intensify through Figure 4n ($\alpha = 14.7°$ on the upstroke, $t/T_{cyc} = 0.85$) before beginning to retract upstream and vector downward slightly in Figures 4o ($\alpha = 15.6°$, $t/T_{cyc} = 0.90$) and p ($\alpha = 16.8°$, $t/T_{cyc} = 0.95$).

In the presence of time-periodic bleed, changes in the wake vorticity and velocity distributions relative to the base flow reveal the mechanism by which abrupt variations in aerodynamic forces and moments are suppressed, resulting in significant improvements in pitch stability while maintaining cycle-averaged forces and moments. Figure 5 shows measurements across the same domain and timesteps as Figure 4 except with time-periodic bleed applied at $St_{act} = 1.1$. Perhaps the most striking difference between Figures 4a and 5a is the cross stream extent to which the CW vorticity layer emanating from the suction surface has spread in the presence of bleed ($\Delta y/c = 0.13$ without and 0.43 with bleed at $x/c = 0$), which produces a domain of recirculating flow $\Delta y/c = 0.15$ thick near the trailing edge and in part causes the lift deficit of $\Delta C_L \approx$ -0.25 discussed in Figure 2a. However, by segmenting the separating shear layer over the airfoil (as discussed in relation to Figure 3b) and thus effectively spreading vorticity concentrations over a wider cross stream area, bleed acts to damp out the shedding of the shear layer vortex that occurs in the base flow (cf. Figure 4c) as well as alleviate the abrupt transition from fully attached to fully separated flow that is observed for the baseline airfoil between Figures 4b and d. The result is a significant improvement in the behavior of the pitching moment: moment stall occurs earlier with bleed ($\alpha = 18.8°$ versus 20.0° for the baseline; cf. Figure 2b); the rate of change of the moment is reduced

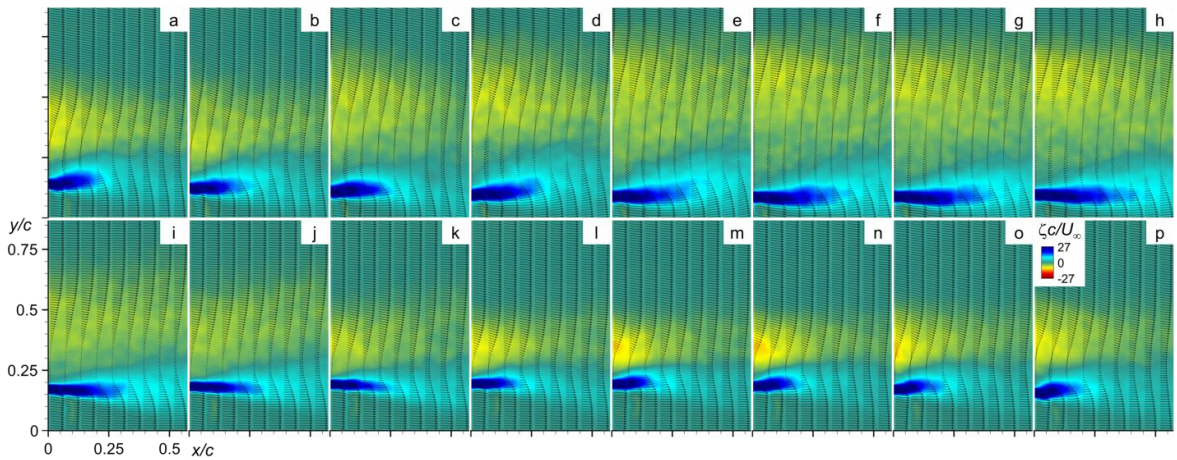

Figure 5*. Same as Figure 4 but in the presence of bleed (*$St_{act} = 1.1$*).*

($dC_M/d\alpha \approx$ -0.08/° versus -0.19/° for the baseline); and the peak magnitude of C_M is reduced ($C_{M,min}$ = -0.30 versus -0.35 for the baseline). Furthermore, no downward vectoring of the CCW shear layer is observed with bleed. Throughout the downstroke, flow appears separated (Figures 5f-j, t/T_{cyc} = 0.25 to 0.65; likewise for the baseline airfoil) although lift levels and rates of change remain higher and lower, respectively, with bleed, contributing to the similar cycle-averaged lift values discussed previously. The reattachment process becomes evident in the wake in Figure 5j (α = 14.8°, t/T_{cyc} = 0.65) as the domain of CW vorticity begins to collapse and the CCW layer begins to retract in streamwise extent. While the levels of C_L in Figure 5l (α = 14.0°, t/T_{cyc} = 0.75) with and without bleed are momentarily equivalent at 1.1 (cf. Figure 2a), the increase in incidence while flow is attached results in a significantly higher rate of change in lift ($dC_L/d\alpha \approx$ 0.96/°) for the baseline airfoil than with bleed ($dC_L/d\alpha \approx$ 0.09/°; cf. Figure 2a), and the cross stream extent of the CW vorticity layer remains wider and its intensity lower than for the baseline through the remainder of the pitch cycle.

The tendency of time-periodic bleed to smooth the abrupt transitions between attached and separated flow experienced by the baseline airfoil during pitching is clearly seen in the variations of cross stream distributions of the streamwise flux of spanwise vorticity through the wake. Figure 6 shows color raster plots of cross stream distributions of vorticity flux $u(x,y,t)\cdot\zeta(x,y,t)$ through the wake (measured 0.3c downstream from the trailing edge using phase-locked PIV) in the absence (a-c) and presence (d-f) of time-periodic bleed taken at 20 equal phase increments during the pitch cycle at rates of k = 0.08 (a, d), 0.17 (b, e) and 0.34 (c, f), beginning at α = 18° on the upstroke. The excursion of the trailing edge is marked on the ordinate. Figure 6a shows that at the quasi-steady pitch rate (k = 0.08), the baseline airfoil initially sheds two distinct opposite-sense vorticity layers between $0.10 < y/c < 0.30$ associated with pressure-side (blue, CCW) and suction-side (red, CW) shear layers. The breakup of the layers begins near t/T_{cyc} = 0.05 when a shear layer vortex sheds into the wake, marked by a near-discontinuity in the CCW flux. The dynamic stall vortex sheds shortly thereafter, between $0.10 < t/T_{cyc} < 0.15$ (i.e., prior to α_{max}), and its signature evident in the rapid increase in the cross stream extent of CW flux with a region of diminished flux (here corresponding to separated flow) between $0.15 < y/c < 0.45$. The band of CW flux remains centered near y/c = 0.65 throughout the majority of the downstroke until t/T_{cyc} = 0.62, when flow abruptly reattaches and the CW band of flux returns to its pre-stall location near y/c = 0.25 while the CCW flux closely tracks the motion of the trailing edge and diminishes in intensity upon flow reattachment.

Bleed produces significant changes to the spatio-temporal structure of the flux through the wake and therefore to the global circulation. Figure 6d shows that at k = 0.08, the abrupt excursion of CW flux between the band centered at y/c = 0.25 (t/T_{cyc} = 0.05) and 0.65 associated with the shedding of the dynamic stall vortex is significantly smoothed. Throughout the cycle, bleed spreads the CW flux across a wider cross stream extent than is evident for the base flow (e.g., for $t/T_{cyc} > 0.60$, $\Delta y/c$ = 0.30 with bleed and $\Delta y/c$ = 0.05 without it),

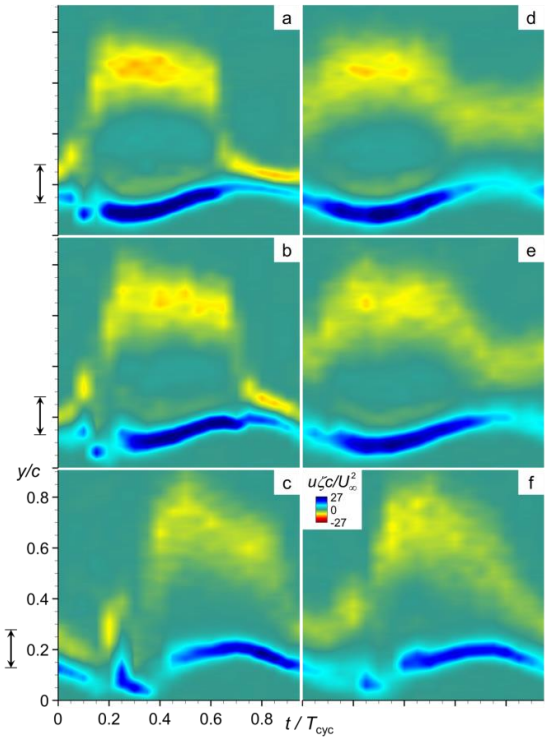

Figure 6*. Cross stream distributions of the streamwise flux of spanwise vorticity during the pitch cycle (derived from phase-averaged PIV measurements taken 0.3c downstream from the trailing edge): k = 0.04 (a, d), 0.17 (b, e), and 0.34 (c, f) in the absence (left column) and presence (right column) of bleed at St_{act} = 1.1. The excursion of the trailing edge is marked on the ordinate.*

indicating that the interaction between the bleed and outer flow discussed in Figure 3 propagates well beyond a limited domain near the bleed outlet and in fact affects the global flow field. Note also that the shear layer vortex that is a precursor to dynamic stall observed in Figure 6a (near t/T_{cyc} = 0.05) is suppressed in the presence of bleed.

The onset of dynamic stall, evidenced by the sharp excursion in cross stream extent in CW flux in part due to the prolonged attachment (stall delay) during upstroke associated with the increased rate of motion, clearly shifts in phase with increasing pitch rate: for k = 0.04, 0.17, and 0.34, onset is visible in the wake domain of the baseline airfoil at t/T_{cyc} = 0.10, 0.18, and 0.34 (Figures 6a-c, respectively). The shedding of the precursor shear layer vortex also becomes more pronounced with k, particularly in the breakup of the CCW layer from $0.1 < t/T_{cyc} < 0.21$ at k = 0.34 (Figure 6c). However, the overall duration of separated flow remains similar (nearly $\Delta t/T_{cyc}$ = 0.50) for each pitch rate. As at k = 0.08, the vorticity flux in the presence of bleed at higher pitch rates (Figures 6e and f) shows significantly more spreading throughout the wake, and the sharp transitions observed between attachment and separation for the baseline airfoil are muted. Although no sharp transition marks the phase of dynamic stall onset, the flux behavior through the wake with bleed appears to lead that of the baseline by $\Delta t/T_{cyc} \approx$ 0.10, which indicates *earlier* shedding of the dynamic stall vortex that in turn reduces the sharp peak in C_L and negative peak in C_M (cf. Figures 2a and b) and thereby increases pitch stability.

These significant changes in vorticity flux through the

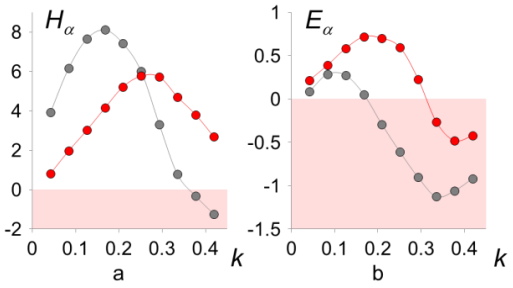

Figure 7*. Variations in the hysteresis coefficient (a, with negative values shaded red) and damping coefficient (b) for time-periodic pitch oscillations (14° < α < 22°) over a range of reduced frequencies: base flow (●) and with time-periodic bleed actuation (St_{act} = 1.1, ●).*

wake due to bleed are manifested as improvements to the cycle lift hysteresis coefficient, calculated as $H_\alpha = \frac{\int C_L d\alpha}{\pi \bar{\alpha}^2}$, as well as to the pitch stability of the baseline airfoil. The overall effects of bleed actuation on the hysteresis and damping coefficients over a range of reduced frequencies (k < 0.42, corresponding to f_{pitch} < 10 Hz) for 14° < α < 22° are demonstrated in Figures 7a and b, respectively. The baseline levels of lift hysteresis coefficient are shown in Figure 7a to increase rapidly to a peak of H_α = 8.10 at k = 0.17 before falling off and even becoming negative beyond k = 0.35. In the presence of bleed, the local maximum in hysteresis (H_α = 5.77) is displaced to k = 0.25 as well as significantly reduced compared to the baseline values for k < 0.25. It is also noteworthy that because a given bleed configuration leverages the time-varying pressure differences between inlets and outlets during pitch oscillations, an increase or decrease in local pressure at the inlet and outlet ports, respectively, can result in an increase in the bleed strength and potentially its effectiveness. As alluded to in connection with Figure 2, the stability of the baseline airfoil decreases significantly with increasing reduced frequency while the regulation of vorticity flux and advection using bleed actuation results in significant stability enhancement. Figure 7b shows the variation of E_α with reduced frequency in the absence and presence of bleed actuation. These data show the base flow is most stable near the quasi-steady range (E_α = 0.29 at k = 0.08) for this range of pitch angles, and thereafter stability diminishes with increasing k, changing sign at k = 0.18 and reaching a minimum of E_α = -1.13 at k = 0.34. However, bleed actuation significantly enhances the pitch stability with increasing k with a peak of E_α = 0.72 at k = 0.17 (in the quasi-unsteady regime) and a change in sign at k = 0.31 (maintaining an average increment of E_α = 0.88 above the baseline for k > 0.21). As discussed in Figures 4 and 5, the timing of the formation and advection of the dynamic stall vortex plays a crucial role in the severity of moment stall, leading to negative damping; by regulating the flux of vorticity from the suction surface, bleed disrupts the dynamic stall vortex and significant improves pitch stability. Though not shown here, bleed actuation is accompanied by small changes ($\Delta C_L/C_{L0}$ ± 5% and $\Delta C_D/C_{D0}$ ± 10%) in the cycle-averaged lift and drag compared to the baseline flow. Of course, the bleed can be further tuned in concert with such changes in the flow, although such optimization was not attempted during the present investigations.

CONCLUSIONS

Distributed active bleed is used to control the aerodynamic forces and moments on an airfoil pitching through its static stall angle (14° < α < 22°) at $k \leq 0.42$ in wind tunnel experiments by altering the strength of vorticity concentrations and the timing of their shedding. Measurements of the spatial and temporal structure of the vorticity flux that is associated with the formation and advection of the dynamic stall vortex show that the modifications due to bleed result in a significant reduction in the abrupt transitions between attached and separated flow. This leads to increased stability ($\Delta E_{\alpha,max}$ = 1.21 at k = 0.25) and reduced lift hysteresis ($\Delta H_{\alpha,peak}$ = 2.33) relative to the base flow, particularly considering the relatively low mass flow rate of the bleed [C_Q is of O(10^{-4})]. *These findings indicate that time-periodic bleed can be used to tailor the damping performance of the airfoil and therefore its vibration and flutter characteristics.*

ACKNOWLEDGEMENT

This work is supported by the Rotorcraft Center (VLRCOE) at Georgia Tech.

REFERENCES

Carta, F. O., "An Analysis of the Stall Flutter Instability of Helicopter Rotor Blades," *J. of the Am. Heli. Soc.*, **12**, 1967, 1-18.

Ericsson, L. E., and Reding, J. P., "Fluid Mechanics of Dynamic Stall Part I. Unsteady Flow Concepts," *J. of Fluids and Structures*, **2**, 1988, 1-33.

Han, Y., and Leishman, J., "Investigation of Helicopter Rotor-Blade-Tip-Vortex Alleviation Using a Slotted Tip," *AIAA J.*, **42**, 2004, 524-535.

Hunter, C.A. Viken, S.A., Wood, R.M., and Bauer, S.X.S., "Advanced Aerodynamic Design of Passive Porosity Control Effectors," AIAA Paper 0249, 39th AIAA Aerospace Sciences Meeting, Reno, NV, 2001.

Johnson, W., and Ham, N. D., "On the Mechanism of Dynamic Stall," *J. of the Am. Heli. Soc.*, **17**, 1972, 36-45.

Kearney, J. M., and Glezer, A., "Aerodynamic Control using Distributed Bleed," AIAA Paper 3246, 6th Flow Control Conference, New Orleans, LA, 2012.

Kearney, J. M., and Glezer, A., "Aero-Effected Control of a Pitching Airfoil by Bleed Actuation," AIAA Paper 2519, 31st Applied Aerodynamics Conference, San Diego, CA, 2013.

Kearney, J. M., and Glezer, A., "Aerodynamic Control of a Pitching Airfoil by Active Bleed," AIAA Paper 2045, 32nd Applied Aerodynamics Conference, Atlanta, GA, 2014.

Lachmann, G., "Results of Experiments with Slotted Wings," NACA TM No. 282, 1924.

Lopera, J., Ng, T. T., and Patel, M. P., "Experimental Investigations of Reconfigurable Porosity for Aerodynamic Control," AIAA Paper 2695, 2nd AIAA Flow Control Conference, Portland, OR, 2004.

McCroskey, W. J., Carr, L. W., and McAlister, K. W., "Dynamic Stall Experiments on Oscillating Airfoils," *AIAA J.*, **14**, 1976, 57-63.

Raghav, V., and Komerath, N., "An Exploration of Radial Flow on a Rotating Blade in Retreating Blade Stall," *J. of the Am. Heli. Soc.*, **58**, 2013, 1-10.